International Journal of Fatigue 165 (2022) 107227

Contents lists available at ScienceDirect

International Journal of Fatigue

journal homepage: www.elsevier.com/locate/ijfatigue

Influence of production batch related parameters on static and fatigue resistance of LPBF produced AlSi7Mg0.6

Stefania Cacace [a], Ali Gökhan Demir [a], Giuseppe Sala [b], Antonio Mattia Grande [b,*]

[a] Department of Mechanical Engineering, Politecnico di Milano, Via La Masa 1, 20156 Milano, Italy
[b] Department of Aerospace Science and Technology, Politecnico di Milano, via La Masa 34, 20156 Milano, Italy

ARTICLE INFO

Keywords:
AlSi7Mg0.6
Laser powder bed fusion
Tensile properties
Fatigue life
MANOVA

ABSTRACT

In laser powder bed fusion (LPBF), the influence material properties are often determined as a function of the inclination with respect to the build direction. In industrial production with variable component shapes and dimensions, the part orientation will often be a matter of the available space in the build volume. Additionally, build-to-build variability is an important factor that may impact the mechanical properties that are often not quantified. Such sources of variability are of great importance for highly demanding sectors such as aviation and aerospace, where lightweight Al-alloys are often used with the geometrical freedom given by the LPBF process. Hence, this work systematically investigates the influence of production batch-related parameters together with part inclination in the LPBF of AlSi7Mg0.6 alloy. Three builds were executed to quantify the impact of the batch, part position, and inclination on the static and fatigue resistance of the alloy in a completely randomized experimental design using an industrial LPBF machine. The results were analysed by the appropriate statistical methods both for discrete and functional data. The results showed that while the part orientation only influenced the static properties, the part position significantly affected the fatigue life demonstrated by the different low cycle fatigue life coefficients.

1. Introduction

Laser Powder Bed Fusion (LPBF) is a metal additive manufacturing technology that enables the manufacturing of complex parts. It promises to improve the mechanical properties of the component while reducing production costs and time [1]. Despite its potential, LPBF technology still needs to demonstrate the capability to produce consistently high-quality parts and provide a robust, stable, and repeatable process [2 3]. Achieving a consistent, high-quality production is challenging in LPBF due to the high number of process parameters involved (up to 100 [4]) and the complex physics behind the process [5]. Extensive studies focused on specific parameters, such as laser-related process parameters [6], scanning strategies [7], post-processes [8] and powder properties [9]. Consequently, certification and qualification of components produced via LPBF become critical, especially for sectors where reliability and safety concerns are of interest, for example, aerospace [10]. Controlling and reducing the variability of the part's mechanical properties is an essential step toward a full qualification and certification of the LPBF process for the aerospace industry. For aerospace production, such variability is often confronted via fresh powder supply at each build job. While such a solution may resolve issues related to powder contamination and damage, it is not sustainable from an environmental perspective. Moreover, the effects of the machine and build variability are not resolved. Indeed, the problem of studying location-related effects and batch-to-batch variability is very complex from an experimental design perspective. The definition and the separation of the variability sources and the number of specimens required require a good understanding of the statistical methods and the LPBF process. In addition, the experimentation should be designed to estimate the effects of these factors independently [11].

Al-alloys are often used in LPBF to produce components in the aerospace industry. AlSi7Mg0.6 alloy is relatively easy to process by LPBF (compared to other aluminium alloys) due to its good fluidity in the molten state and the slight difference between its liquidus and solidus temperatures. On the other hand, compared to steels and titanium alloys, its production using this powder bed technique can be problematic due to its high reflectivity and high thermal conductivity and the formation of oxide layers on the melt pools [12,13]. While the Al-Si-Mg alloy family is widely used in LPBF, only a limited number of works regarding the processing of AlSi7Mg0.6 are present in the literature.

* Corresponding author.
E-mail address: antoniomattia.grande@polimi.it (A. Mattia Grande).

https://doi.org/10.1016/j.ijfatigue.2022.107227
Received 18 March 2022; Received in revised form 22 August 2022; Accepted 23 August 2022
Available online 28 August 2022

Commonly the effect of the process parameters and heat treatments on the tensile and fatigue properties have been reported. Rao et al. [14] showed that the fast-cooling rate of the process leads to a very fine microstructure that influences the mechanical properties of the samples along with the process parameters selected. Rao et al. [13] investigated the effect of the heat treatments showing improved tensile ductility and reduced tensile strength compared to the cast counterparts. Aversa et al. [15] studied the impact of the build platform temperature on the mechanical properties showing that in-process ageing was possible through the correct temperature setting. Trevisan et al. [16] investigated the effects of stress-relieving treatment, followed by T6 treatment, showing the necessity to combine the two stages for parts without deformations and adequate mechanical properties. Saravana et al. [17]investigated the effect of print orientation on mechanical properties, showing how this parameter affects this alloy's static and fracture response. In contrast, Bassoli et al. [18]studied the fatigue response in as-built conditions. Only recently, the influence of powder reuse has been investigated where a general reduction of the mechanical properties was observed with Al-alloys [19]. The results show that the Al-alloys are highly sensitive to the process's thermal fields and the post-processing conditions. Such sensitivity underlines the need for a better understanding of the uncontrolled factors between batches.

Only a few works in literature attempted to investigate the batch-to-batch variability issues in LPBF. Soltani-Tehrani et al. [20] studied the effect of sample location on the static and dynamic properties of the 17-4PH alloy. They found that location was negligible for tensile properties, while the fatigue properties of the machined samples decreased as the powder was re-used. Wang et al. [21] did not find a relationship between part location and tensile properties of Hastelloy X. Zhang et al. [22] investigated the effect of location, energy density, and orientation on the tensile properties of Ti6-Al4-V alloy. They found that location was significant and its interaction with the orientation. All the present works tackle the batch-to-batch variability from a single perspective, whereas the need for appropriate experimental designs and adequate statistical tools is apparent. To the authors' knowledge, a systematic investigation that incorporates batch-to-batch variability, part orientation, and position influences on the mechanical properties is still missing.

Accordingly, this work provides extensive experimentation explicitly designed to study the impact of sample location, sample orientation, and build-to-build variability in the LPBF of AlSi7Mg0.6 alloy. A complete factorial experimental design was executed in 3 batches with complete randomization. Static and fatigue properties were measured and analysed via dedicated statistical tools. Analysis of variance (ANOVA) was used to determine the impact of orientation, build-to-build variability, and location on tensile properties. Multi-variate analysis of variance (MANOVA) was instead used to investigate the effect of orientation and location on the estimated S—N curves for fatigue life assessment.

2. Materials and methods

2.1. Experimental procedure

The material used in this study was gas atomized AlSi7Mg0.6 powder (LPW Technology ltd). The particle size of the powder was in the range of 26–66 μm in diameter, and the mean diameter was 41.2 μm.

The LPBF industrial system used in this work was Renishaw AM250. The machine is equipped with a 200 W fiber laser working in pulsed mode and a spot diameter of 75 μm. All builds were carried out under constant Argon flow keeping the oxygen content < 1000 ppm, without platform preheating. The process parameters selected for the sample production were optimized in a previous experimental campaign [23]. The meander scanning strategy was employed, and all the parameters for the fabrication are listed in Table 1. The same powder batch was used throughout the process, where approximately 50 % of the powder used in each build job was recovered from the previous build job. All specimens were stress relived at 300 °C for 2 h.

Table 1
Process parameters used for sample production.

Parameter	Volume	Border
Power, P	200 W	200 W
Exposure time, t	131 μs	140 μs
Point Distance, d_p	80 μm	80 μm
Hatch distance, d_h	139 μm	n/a
Number of borders	n/a	2
Border distance	n/a	70 μm
Layer thickness, z	25 μm	25 μm
Volumetric Energy density, VED	94 J/mm^3	200 J/mm^3

2.2. Density and surface roughness

Apparent density and surface roughness were measured for all samples before mechanical testing. Then, fatigue specimens were sandblasted manually until the surface roughness was lower than 10 μm to comply with the standard for fatigue testing.

The apparent density of the samples was measured using an electronic scale with a kit for density measurement (Sartorius YDK01) according to Archimede's principle. All measurements were replicated three times, and during the measurement, the water temperature was monitored continuously.

Average surface roughness (Ra) was measured using a tactile roughness measurement instrument (Perthometer S6P). The acquisition length was 12 mm, with a 0.8 mm cut-off length. Due to the presence of supports, the surface roughness of the samples is not homogeneous in all directions, and this is especially true for horizontal and 45° samples. For this reason, Ra was measured in four directions obtained by rotating the sample approximately 90°along its axis. The measurements along the four reference directions were averaged and analysed. Specimens were measured first as-built and after sandblasting. The sandblasting duration was experimentally evaluated to obtain a final average surface roughness lower than 10 μm on all the measured sides. The surface roughness evolution was assessed by applying sandblasting with intervals of 30 s. The final procedure involved a sandblasting duration of 210 s.

2.3. Mechanical testing

Tensile tests were carried out according to ASTME8/E8M-16a standard. Tensile tests were conducted using an MTS 810 Material Test System machine with a constant strain rate of 0.45 mm/min. A 20 mm extensometer (MTS Model 634.31F-24) was used to measure the axial strain of the specimens. Axial force-controlled fatigue tests were performed to obtain the fatigue strength of the materials selected in this study. Fatigue tests were performed according to the ASTM E466 standard. The experiments were limited to testing axial unnotched specimens subjected to constant amplitude periodic forcing function in air at room temperature. Fig. 1 illustrates the geometry of tensile and fatigue specimens.

The fatigue tests were performed at R = 0.1 using a 20 Hz sinusoidal waveform under load control to a maximum of 10^7 cycles. The R = 0.1 value corresponds to a tension–tension cycle in which the minimum stress is equal to 0.1 times the maximum stress. The geometry of the specimens was selected according to the ASTM E466 standard; the diameter of the test section was set at 6 mm, and the test section length was set at 18 mm. Fatigue tests were carried out in the low cycle fatigue range (about 10^4 cycles) and high cycle fatigue range (>10^5 cycles). Run-out is fixed to 10^7 cycles. Experiments were performed at fixed stress levels in the low cycle fatigue range based on static tensile results (e.g., 80 %, 60 %, and 40 % of the yield stress). The number of fatigue specimens tested at each stress level for each condition was fixed to 4. The total number of specimens for a single S—N curve required to evaluate the material's endurance in the low cycle range was 12. Additional 8 specimens for high-cycle fatigue testing were added for each experimental condition. The staircase method (ASTM E468) is

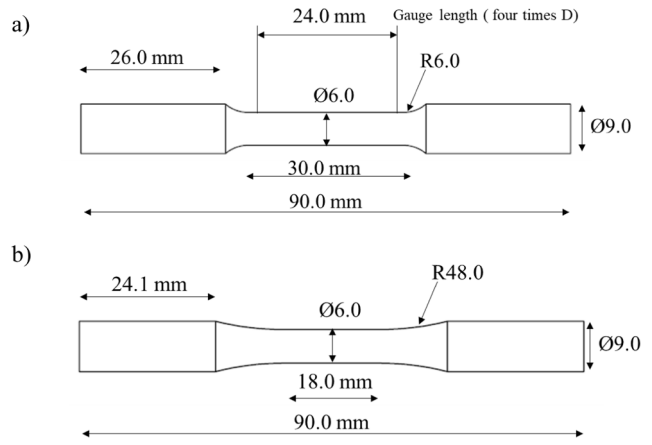

Fig. 1. a) Tensile specimen geometry (ASTM E8) b) Fatigue specimen geometry (ASTM E466).

adopted to determine the statistical properties of the fatigue limit.

Following this method, the first specimen is subjected to a stress corresponding to the expected average fatigue strength. If the specimen survives 10^7 cycles (run-out), it is discarded and the next specimen is subjected to a stress that is one increment above the previous, the stress increment was set at 25 MPa. When a specimen fails prior to reaching 10^7 cycles, the obtained number of cycles is noted, and the next specimen is subjected to a stress that 25 MPa below the failed one. In that way, each test depends on the previous test results and the experiment continues in this manner in sequence with the stress level being increased or decreased until all 8 specimens are tested. Therefore, the total number of fatigue specimens was 20 (12 for low cycle fatigue and 8 for high cycle fatigue). Scanning Electron Microscope (Hitachi TM3000) was used to investigate the causes of fatigue failure using a backscatter diffraction detector and correlate them with the result of the statistical analysis. For horizontal specimens, SEM images were used to measure the size of the critical defects. The area of the defects was evaluated using an image processing routine via MATLAB.

Table 2 summarizes the testing conditions for fatigue experiments. Low cycle fatigue experiments were carried out in random order. A linear regression equation based on the standard formulation was sought using the results. The final number of cycles to failure (S—N) curves was determined by the results of the design of experiments showing the significance of the investigated factors. All specimens were tested after stress-relieving and sandblasting.

Table 2
Details of the fatigue testing procedure.

General	
Stress ratio	R=0.1
Frequency	20 Hz (minimum)
Run-out	10^7 cycles reached by at least three specimens
Low cycle fatigue (10^4 to 10^6 cycles):	
Specimens for each stress level	4
Stress levels	3 Proportional to the static YS e.g., 80%, 60% and 40% of YS
High cycle fatigue (>10^6 cycles)	
Specimens to determine the fatigue limit	8
Max stress increment	25 MPa

3. Experimental design to investigate part position over multiple build jobs

The influence of the location of the samples was assessed by defining two distinct regions, defined as internal and external, as shown in Fig. 2. For the LPBF machine, the internal region was expected to be more favorable for the gas flow and the powder recoating homogeneity. In contrast, external regions can suffer from the non-optimal gas flow and powder layer variations. In addition, the specimens were built according to three different directions concerning the build plate (horizontal, inclined, and vertical) to study the effect of orientation on the tensile and fatigue properties. Inclined specimens refer to a building direction of 45° with respect to the building platform.

A total of 6 different combinations existed for testing: two levels of position (internal and external) and three different orientations (vertical, inclined, and horizontal). For each combination, five tensile specimens and 20 fatigue specimens were produced. The specimens were produced in 3 different batches to evaluate the batch-to-batch variability. The specimens were fully randomized over the three builds to avoid blocking effects on the analysis [11]. The presence of a non-detected blocking impact could affect the investigation. For this reason, it is essential to distribute the specimens randomly to avoid systematic errors. Accordingly, 40 fatigue and 10 tensile specimens were placed on each build plate. The distribution of the specimens over the three builds is reported in Table 3 and Fig. 3. The specimens are built-in net shape and sand-blasted, as described in Section 2.3.

Support structures were added to all the surface specimens with an inclination angle of<45°. In particular, the vertical specimens had no supports on the calibrated region of the test geometry. The supports of inclined specimens were designed to be minimally invasive and reduce their effect on surface roughness and, therefore, fatigue properties. The horizontal specimens had to be supported along the downfacing surfaces, potentially leaving support marks on the calibrated region of the specimens. Static tensile properties were analyzed via ANOVA (analysis of variance) with a statistical significance level p-value of 5 %. S—N curves resulting from the low-cycle fatigue testing were instead analyzed using MANOVA to assess the influence of position and location on the fatigue properties.

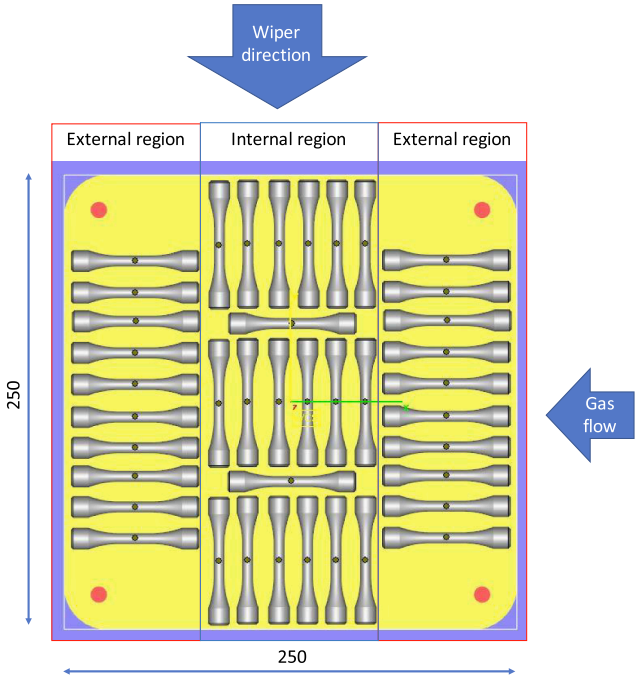

Fig. 2. Definition of internal and external position on the building platform. The arrows show the gas flow direction and the powder wiper direction.

Table 3
Random distribution of the fatigue and tensile specimens over the three build plates.

Build no	Orientation	Position	No fatigue specimens	No tensile specimens
1	Vertical	External	6	1
		Internal	6	1
	Inclined	External	8	3
		Internal	7	2
	Horizontal	External	7	2
		Internal	6	1
2	Vertical	External	6	2
		Internal	8	2
	Inclined	External	8	0
		Internal	4	2
	Horizontal	External	6	2
		Internal	8	2
3	Vertical	External	8	2
		Internal	6	2
	Inclined	External	4	2
		Internal	9	1
	Horizontal	External	7	1
		Internal	6	2
Total			120	30

Six S—N curves were estimated from the low cycle fatigue data (12 specimens), one for each combination of orientation and position. The objective of the analysis is to evaluate the effect of these two factors on the fatigue response. ANOVA could not be used as the output of the fatigue experiment is a curve. MANOVA is a generalization of ANOVA where multi-dimensional variables are considered a response [24], which was used to assess the influence of position and location on the coefficients of the S—N curves.

The model for the estimation of the S—N curves was the following:

$$\log_{10}N = \beta_0 + \beta_1 \log_{10}S + \varepsilon \quad (1)$$

where β_0 and β_1 are the regression equation coefficients, and ε is the error term with $\varepsilon \sim N(0, \sigma^2)$. The objective of the analysis was to determine if these two factors influenced the fatigue life of AlSi7Mg0.6 samples estimated as in Eq (1). In this work, the response of the analysis was the vector of the coefficients of the S—N curves. The model used for the study is the following:

$$\boldsymbol{Y}_{ij} = \boldsymbol{\mu} + \boldsymbol{\alpha}_i + \boldsymbol{\gamma}_j + \boldsymbol{\varepsilon}_{ij} \quad (2)$$

where $\mathbf{Y}_{ij}$ is the vector of the coefficients for the six curves, $\boldsymbol{\mu}$ is the overall level, $\boldsymbol{\alpha}_i$ is the effect of the orientation on the response, $\boldsymbol{\gamma}_j$ is the effect of the position on the response, and $\boldsymbol{\varepsilon}_{ij}$ is the error term. To determine if the two factors (orientation and position) are significant, i.e., they affect the coefficients of the regression equation, Wilks statistics were used.

$$\Lambda^* = \frac{|\boldsymbol{E}|}{|\boldsymbol{E} + \boldsymbol{H}|} \quad (3)$$

where **E** is the matrix sum of squares of the error and H is the matrix sum of squares of the model. The significance of the effects of the factor is evaluated based on an approximation of the Fisher Distribution [24]. The p-value associated with the Wilks statistics was compared with a reference value (type I error) equal to 0.05. Hence, if the p-value is lower than 0.05, the factor statistically impacts the response.

4. Results

4.1. Density and surface roughness

The results of the density measurements are shown in Fig. 4. The apparent density varies from 98.8 % to 99.1 %, using a reference density for AlSi7Mg0.6 alloy equal to 2.68 g/cm^3. The mean apparent density of

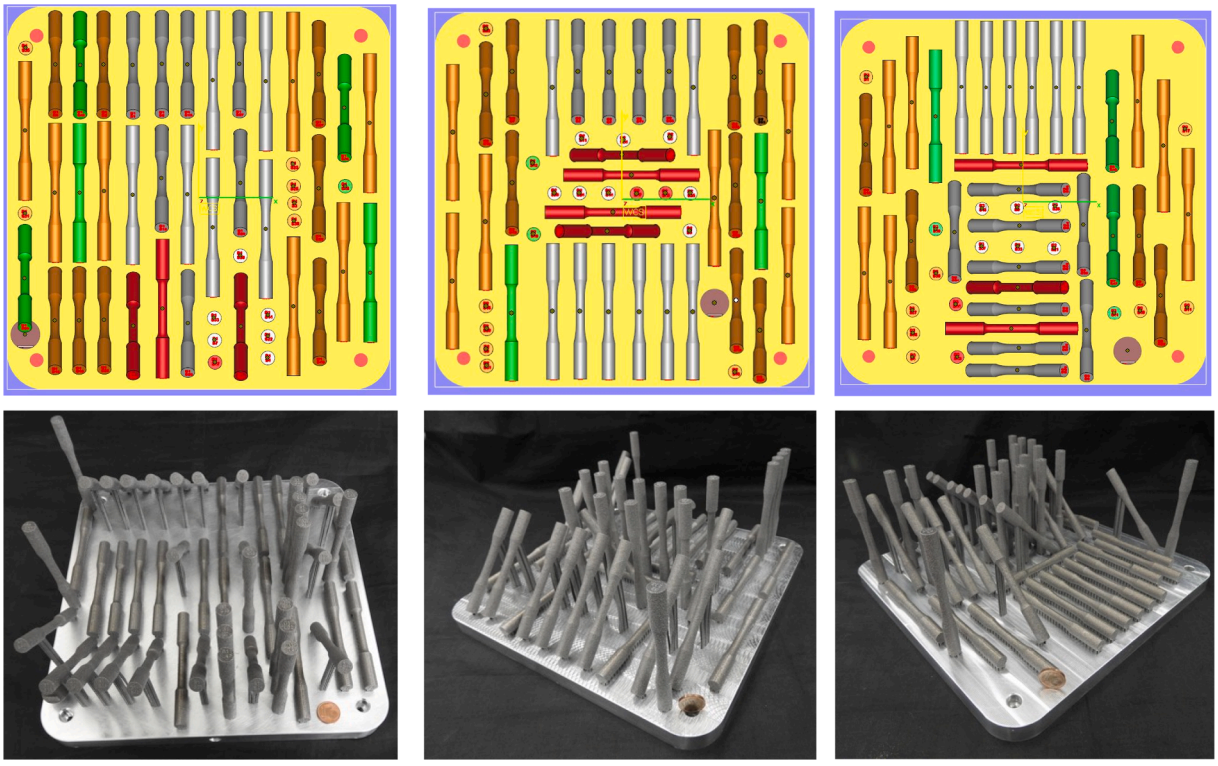

Fig. 3. Distribution of the specimens on the build plate. The specimens follow a specific color code. Gray: Internal fatigue. Red: Internal, tensile. Orange: External fatigue. Green: External, tensile. Build platform size is 250 mm × 250 mm. (For interpretation of the references to color in this figure legend, the reader is referred to the web version of this article.)

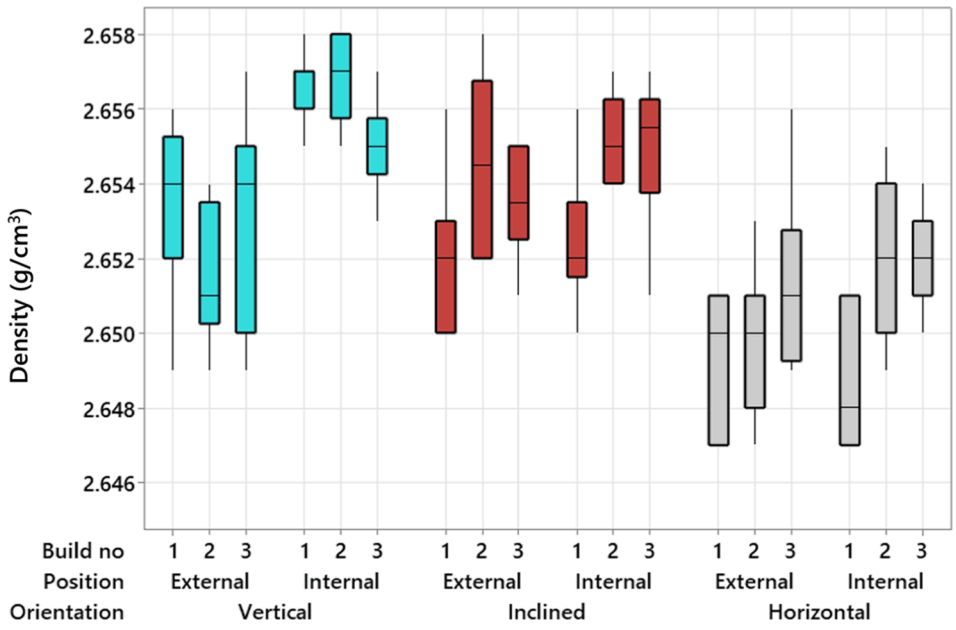

Fig. 4. Density results of tensile and fatigue specimens at different orientations and positions.

samples produced in the internal position is 2.656 ± 0.001 g/cm^3, for the external is 2.653 ± 0.003 g/cm^3, while the apparent densities for the three batches are 2.651 ± 0.002, 2.652 ± 0.003, and 2.653 ± 0.002 g/cm^3, respectively. The samples with horizontal orientation show a slightly lower density, which could be attributed to their higher surface roughness, affecting the measurement accuracy. These results imply no influence of part position or batch on the part density.

Fig. 5 shows the surface roughness measurements. The as-built surface roughness was at Ra < 10 µm for vertical and inclined (45°) samples. However, horizontal samples showed higher surface irregularities, mainly due to the presence of the supports. Therefore, it was necessary to perform sandblasting on all samples to obtain the surface quality required for the fatigue tests. Fig. 5 a) shows that 210 s of manual sandblasting allowed all parts to reach the desired surface roughness value with a wide margin.

Fig. 5 b) illustrates the overall mean surface roughness data after sandblasting. The general surface average roughness is 5.70 ± 0.46 µm. The slight absolute variation of surface roughness among the samples indicates that orientation, build, and location did not influence the surface quality of the samples.

4.2. Tensile properties

The results of the tensile properties are summarized Table 4 and illustrated in Fig. 6. As-built mechanical properties were analyzed in previous work [25]. A horizontal reference line was added to compare the results with the literature ([13;26]). The variations for ultimate tensile strength (UTS), yield strength (YS), and Young's modulus (E) were negligible, considering part orientation, part position, and batch. Instead, elongation at break was characterized by considerable variability.

UTS, YS, and E values of as-built and stress-relieved specimens were coherent with the literature results [13,26]. In general, for these responses, the influence of orientation and position on the building

Table 4
Summarized tensile properties of AlSi7Mg0.6 samples.

Condition	UTS (MPa)	YS(MPa)	E (GPa)	e (%)
As-built	413±1.0	222±1.9	64±1.6	11.0±1.4
Stress relieved	254±5.1	170±4.0	66.9±2.6	13.2±2.3

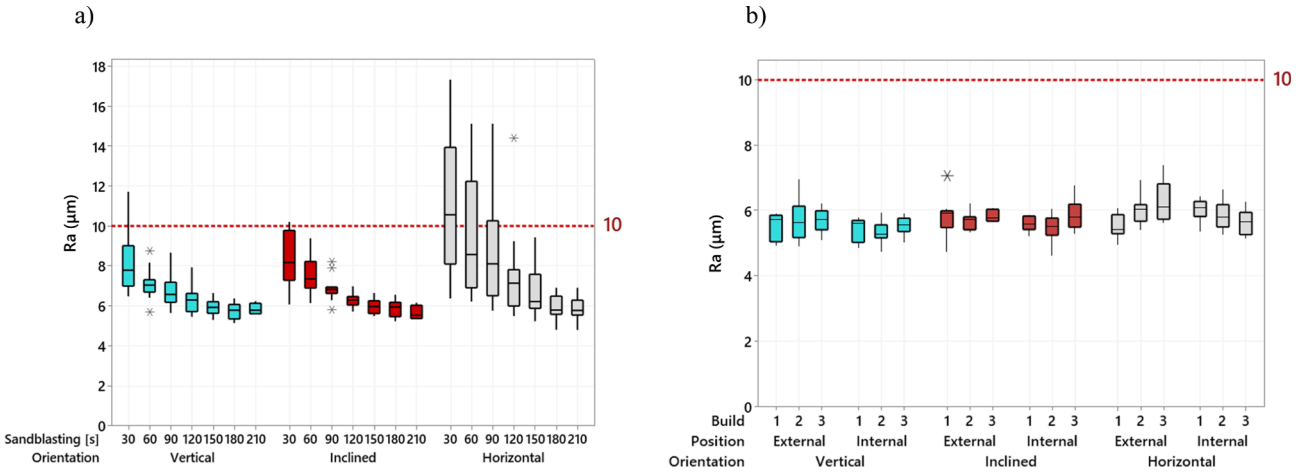

Fig. 5. a) Variation of surface roughness with increasing sandblasting times. b) Average surface roughness as a function of the investigated parameters at the end of the sandblasting process (* indicates potential outlier concerning the group).

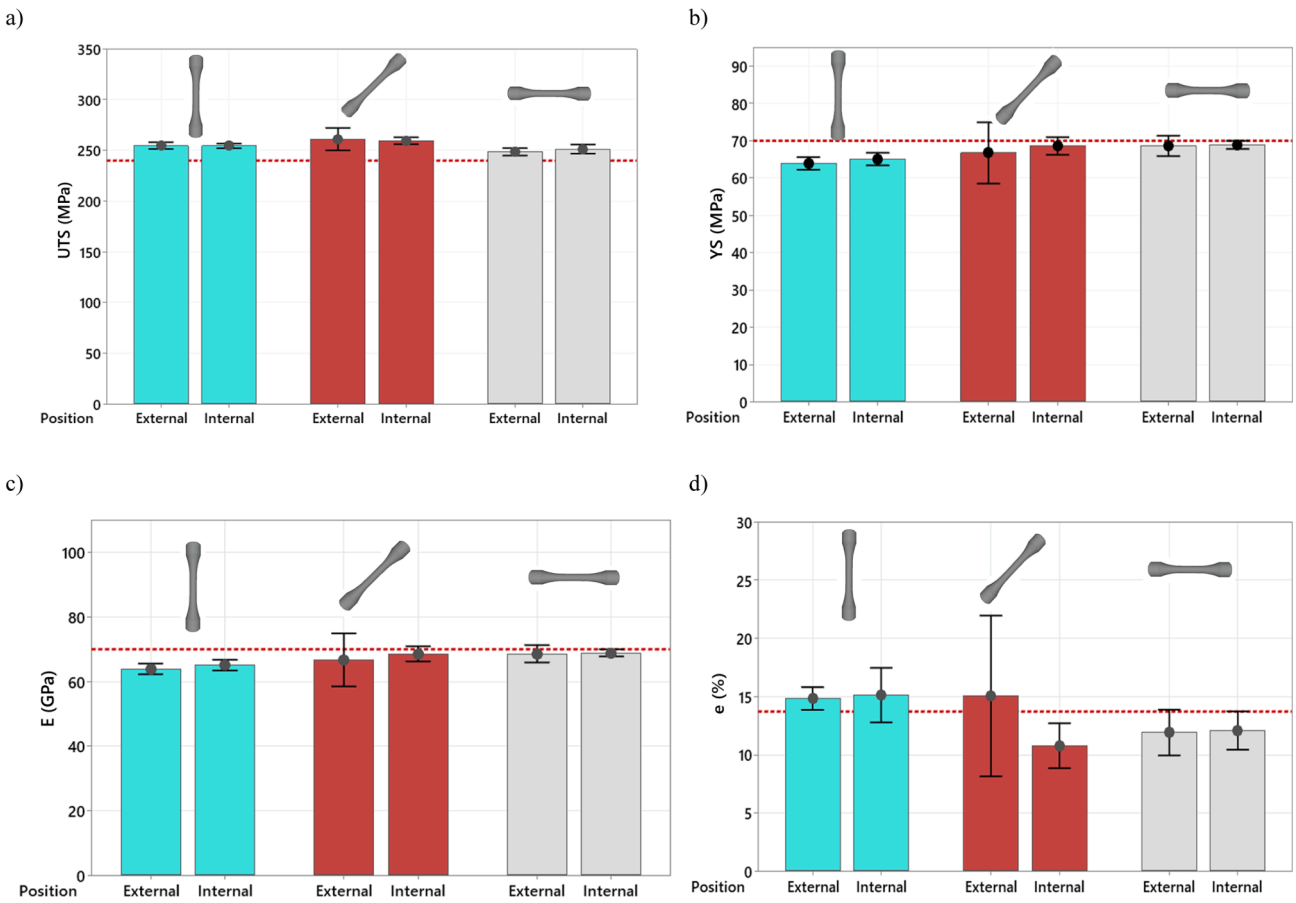

Fig. 6. Tensile properties of AlSi7Mg0.6 alloy after stress-relieving treatment. Reference values are shown as a horizontal line and were based on values found in the literature ([13,26]) a) Ultimate tensile strength, UTS b) Yield strength, YS, c) Young's modulus, E d) Elongation, e.

platform is not visible in Fig. 6. UTS, YS, and Young's modulus values are 254 ± 5.1 MPa, 170 ± 4.0 MPa, and 66.9 ± 2.6 GPa, respectively. Samples built in the horizontal position and at 45° show, a slightly decreased elongation compared to vertical ones. On the other hand, the part position did affect the elongation.

Data displayed in Fig. 6 d) show that vertical samples have the largest elongation, followed by 45° samples, and the least elongation is obtained for horizontal samples; the respective values are 15.0 % ±1.4 %, 12.4 %±2.9 %, and 12.0 ± 1.4 %. Inclined samples in the external position show a much larger variability due to two outliers, resulting in reduced elongation values (1.28 % and 2.69 %). However, considering the overall elongation, the experimentation results are comparable with the reference value (13.6 %).

An ANOVA analysis is conducted to assess the influence of orientation, position, and build and their interactions on the tensile properties, while the results are reported in Table 5. The p-values indicate that orientation is significant for all responses. However, the effects of the overall variability already discussed suggest that these differences are not significant from a practical point of view. Furthermore, the ANOVA results show that the build number and part position and their interactions do not influence the tensile properties.

Table 5
The p-value of position, build-to-build variability, and orientation on the tensile properties based on ANOVA results.

Factors	UTS	YS	E	e
Position	0.784	0.413	0.208	0.124
Build	0.381	0.019	0.544	0.572
Orientation	0.000	0.000	0.000	0.016
Build*Orientation	0.518	0.197	0.257	0.690
Build*Position	0.354	0.073	0.525	0.885
Orientation*Position	0.534	0.332	0.894	0.105

4.3. Fatigue behaviour

Fatigue data for high-cycle and low-cycle analysis are shown in Fig. 7. The plot shows the maximum applied stress versus the cycles to failure for all six combinations of orientation and position. S—N curves were fitted to low-cycle fatigue data points according to Eq. (1), while high-cycle fatigue run-out experiments indicated filled squares or circles. The experimental data follow a well-behaved typical S—N curve shape on a logarithmic scale. In general, shorter fatigue lives were observed for horizontal specimens, while vertical and inclined ones exhibited longer fatigue lives.

The coefficients of the six S—N curves are shown in Table 6, along with the resulting Mean Square Error (MSE). The coefficients are shown in coded units to allow easier comparison between the curves. In addition, for each regression curve, the hypotheses on the residuals (normality and homogeneous variance) were verified. In the last column of Table 6, the run-out results of high-cycle fatigue are reported as mean stress ± 1 standard deviation, σ.

The standard deviation for High Cycle Fatigue is based on only 8 specimens, that is a small sample. These 8 samples were spread uniformly on the three builds and the resulting value of standard deviation can be therefore considered as a worse-case scenario. The values of standard deviations derived from the present experiment are coherent with the ones obtained by other authors for Al-alloys [27,28].

The results show that both position and orientation influence low cycle fatigue. However, the effect of position is negligible. An important aspect is the MSE of the regressions, where the higher the MSE

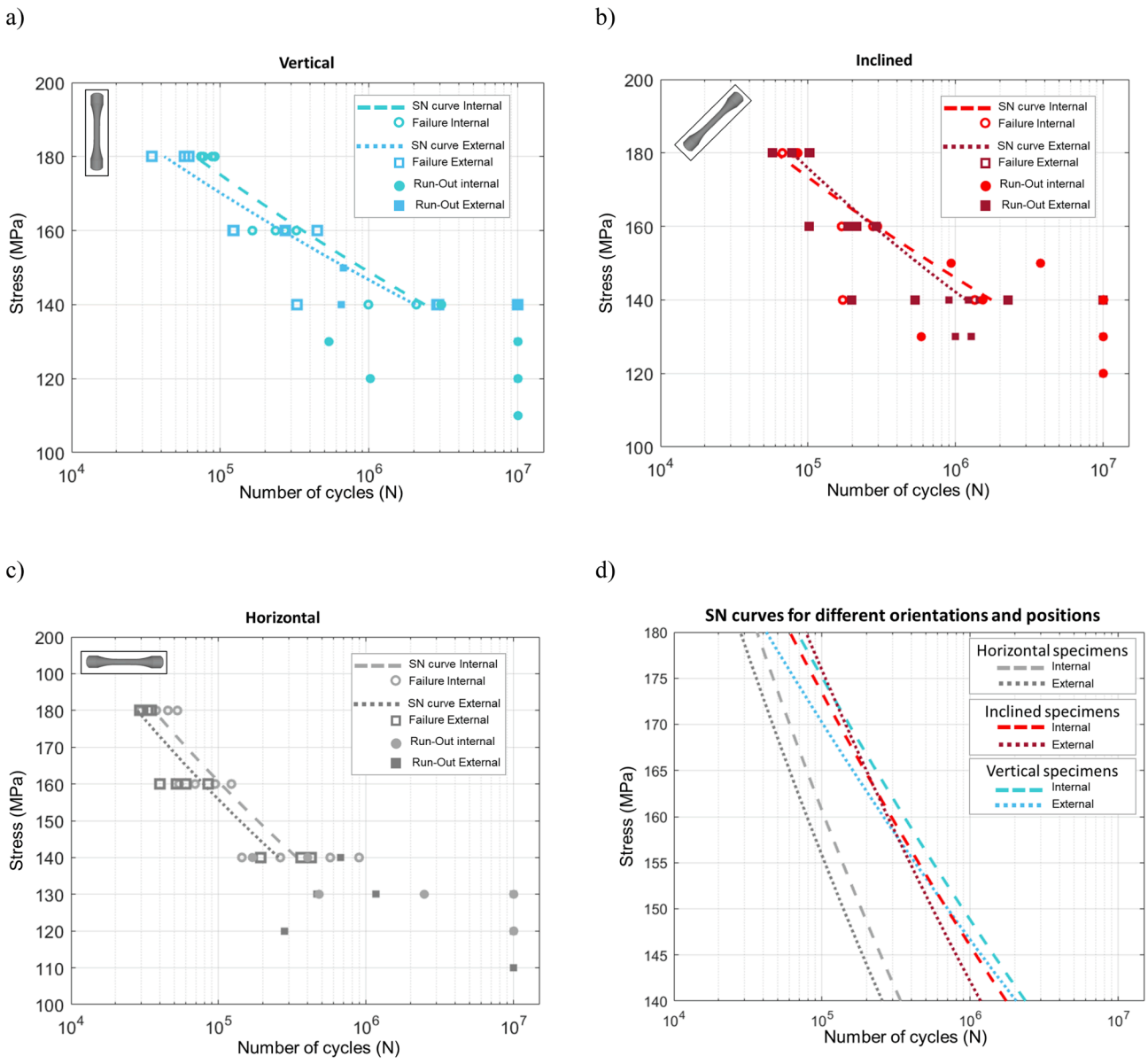

Fig. 7. S—N diagram for low cycle fatigue tests. S—N curves are reported for internal and external samples for each orientation a) vertical, b) inclined, c) horizontal, and d) comparisons of the estimated curves.

Table 6
Fatigue properties of AlSi7Mg0.6 as a function of orientation and position.

Orientation	Position	EquationLow cycle fatigue	MSE	Run-out (±1σ) High cycle fatigue
Vertical	Internal	$\log_{10}$ N= 5.60 - 0.77 $\log_{10}$ S	0.07500	122±8.4 MPa
	External	$\log_{10}$ N= 5.47 - 0.84 $\log_{10}$ S	0.16390	132±8.4 MPa
Inclined	Internal	$\log_{10}$ N= 5.56 - 0.73 $\log_{10}$ S	0.25090	132.5±9.6 MPa
	External	$\log_{10}$ N= 5.44 - 0.59 $\log_{10}$ S	0.19230	127.5±5.0 MPa
Horizontal	Internal	$\log_{10}$ N= 5.04 - 0.49 $\log_{10}$ S	0.05396	125±5.8 MPa
	External	$\log_{10}$ N= 4.92 - 0.48 $\log_{10}$ S	0.02757	120±10.0 MPa

corresponds to the higher variability. The 45° samples showed a larger variability of the results, especially for the internal position. For vertical samples, the lowest MSE is obtained for internal samples, while the lowest variability is obtained in the external condition for the horizontal orientation. The effect of orientation and position on the variability of the fatigue life data is not clear.

The MANOVA table for the two coefficients (β_0 and β_1) is reported in Table 7. The R^2_{adj} of the two models is 99.9 % and 95.6 %, respectively. A weighted analysis was carried out using weights 1/MSE of the individual models to account for the different variability in the estimates of the

Table 7
Influence of orientation and position on the coefficients of the SN curves using p-values from MANOVA analysis.

	β_0		β_1	
Source	F-value	p-value	F-value	p-value
Orientation	7335.71	0.000	21.03	0.045
Position	762.12	0.001	0.01	0.928

regression equations (MSE in Table 6). The hypotheses of MANOVA (normality and homogeneous variance of the residuals) were checked. The result shows that the intercept β_0 is influenced by both position and orientation (p-values lower than 0.05), while the coefficient β_1 is affected only by the orientation (p-value equal to 0.045 < 0.05). The mean value of the coefficients and for each level of orientation and position, shown in Table 8, were used to assess the differences between the mean groups at the different levels of Orientation and Position. Orientation largely influences the intercept β_0 by reducing its value from 5.54 for the vertical samples to 4.98 for the horizontal samples. On the other hand, position affects β_0 but to a smaller extent. A low intercept value indicates that horizontal samples sustain less stress than vertical and inclined ones. However, most of the literature is based on machined samples, where the influence of the surface quality with different inclinations may not be evaluated.

According to Sanaei and Fatemi [29], rough surfaces are the primary source of fatigue failure, while microstructure and internal defects have a secondary effect, stronger after longer fatigue life [37]. A reduced fatigue life characterizes horizontal samples because of the massive presence of supports which increase the surface roughness of the samples and could result in stress concentrations on the surface [38]. This conclusion is supported by the fracture analysis carried out in the following. Orientation was also found to influence the coefficient β_1. The coefficient β_1 was smaller for horizontal samples and larger for vertical ones. Vertical samples sustained higher stresses than the horizontal samples (large β_0), but they possessed a faster reduction in fatigue life as the applied stress is increased (large β_1). This result indicates that as stress is increased, the effect of orientation on fatigue life is reduced due to the greater sensitivity to defect size and position rather than surface quality.

The position of the samples influenced only the intercept as internal samples sustain higher stresses than external ones (β_0 is 5.4 for internal samples and 5.28 for external ones). The higher mechanical properties of internal samples over external ones were expected due to the influence of the gas flow [39]. The fatigue life was reduced by the same amount as stress is increased independently of the location (the coefficient β_1 is the same). However, the differences seem to be relatively small compared to the effect of the orientation and might be due to the inevitable other uncontrolled variability sources.

In conclusion, the statistical analysis revealed that horizontal samples tend to have low fatigue properties compared to inclined and vertical samples. However, the coefficient β_1 is larger for vertical and inclined samples, indicating that fatigue decreases more sharply in these orientations than in the horizontal samples. The position on the platform had a mild influence on the intercept (p-value 0.045), with internal samples characterized by improved fatigue properties.

The lowest average fatigue limit was obtained for the horizontal samples built in the external position. Also, horizontal specimens tended to show the worst behavior in the region of high-cycle fatigue. There is only one exception to this trend. In the vertical samples, the external position resulted in a low fatigue limit (122 MPa), close to horizontal samples in both positions (125 MPa for internal and 120 MPa for external). In general, the average fatigue limit resulting from the staircase method shows a slight variation among the three orientations and the two positions. Still, it appears that vertical and inclined specimens present slightly higher properties.

Table 8
Differences in the coefficients of the SN curves at each level for orientation and position.

Orientation	β_0	β_1
Vertical	5.54	-0.79
Inclined	5.50	-0.65
Horizontal	4.98	-0.48
Position	**β_0**	**β_1**
Internal	5.40	-0.64
External	5.28	-0.64

We can draw the following practical conclusions for Low Cycle Fatigue data:

- The position of the sample on the platform has minor effect on the cycles to failure for a given stress level, as visible in Fig. 6 d). For a given orientation, the internal and external curve are almost parallel for vertical and horizontal specimens, and for these orientations external specimens show reduced fatigue properties. On the contrary inclined specimens show conflicting results, with internal specimens resulting in higher fatigue life at high stress levels; however, the external position sees a faster reduction of fatigue properties as the stress level is reduced.

- The effect of the orientation on the cycles to failure increases as the stress level is increased. At low stress levels, the difference between vertical and horizontal specimens is large, the mean cycle to failure is $4.02x10^6$ for vertical specimens and $9.6x10^5$ for horizontal ones. At high stress levels this difference is highly reduced, with vertical specimens resulting in $7.8x10^4$ mean cycle to failure while for horizontal ones the result was $3.7x10^4$.

These differences should be considered by the designer especially when dealing with aerospace applications where complex geometry are required and all sources of variability need to be accounted for design and qualification purposes. The fracture analysis presented supports the statistical analysis explaining the fatigue behavior of AlSi7Mg0.6 specimens.

4.4. Fracture analysis

The features responsible for the crack initiation were investigated using backscatter SEM images. Examples of the primary defect types: lack of fusion (irregular shape) and spatter (characterized by round shape) induced pores are illustrated in Fig. 8.

Fig. 9 shows representative fractography images of post-mortem fatigue specimens. All fracture surfaces exhibited an initiation site from defects, a stable crack propagation region, and a fast fracture region. In Fig. 9, the critical flaws that caused failure are indicated with a red circle. Vertical and inclined specimens failed due to surface or subsurface defects, while most of these flaws were characterized by unmelted particles. The position of the initiation site for vertical and inclined specimens could neither be correlated with the presence of the supports (for inclined specimens) nor with the position of the sample on the platform. The crack initiation defect for vertical and inclined specimens was located on the surface. Un-melted particles were frequently observed, which may be caused both due to lack of fusion and spatter-induced lack of adherence. Such sub-surface defects may be related to the chosen border parameters [40], which were not varied throughout this work. Lack of fusion around the border region can also be induced due to an incomplete overlap between volume and border scan lines. Such conditions may also arise from the discrete number of scan lines applied to the complex shapes [41]. Essentially around the border, the volume scan lines may be missed due to the skipping of a very short scan vector. Multiple border scan lines may help reduce such issues by increasing the production time. Indeed, finishing methods may improve the fatigue life of Al-alloys [42]. If machining is used on the parts, the machining allowance should be larger than the border thickness to avoid sub-surface defects.

Differently, the initiation site of all horizontal specimens corresponds with the support area. All the samples were previously sandblasted and stress-relieved. It is known that during the LPBF of Al-alloys, thermal gradients may be sufficiently large to cause part deformations or internal stresses [43]. Horizontal specimens are more prone to such issues, where stress-relieving processes may not always be sufficient.

The magnified SEM images in Fig. 9 clearly show the rough surface of the horizontal specimens where the fatigue crack started, suggesting that the surface quality had a major impact on the fatigue failure for this orientation. In addition, the size of the initiation site was much larger for

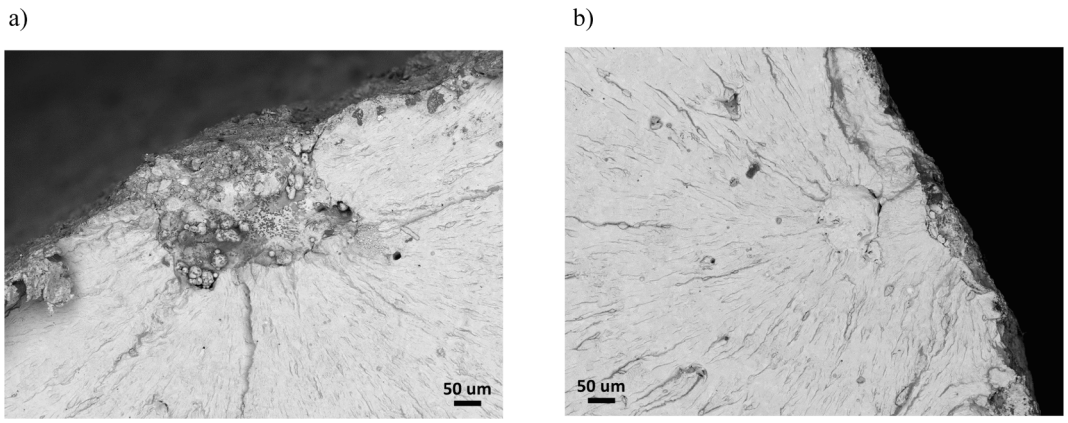

Fig. 8. SEM backscatter image of typical defects. a) lack of fusion b) spatter.

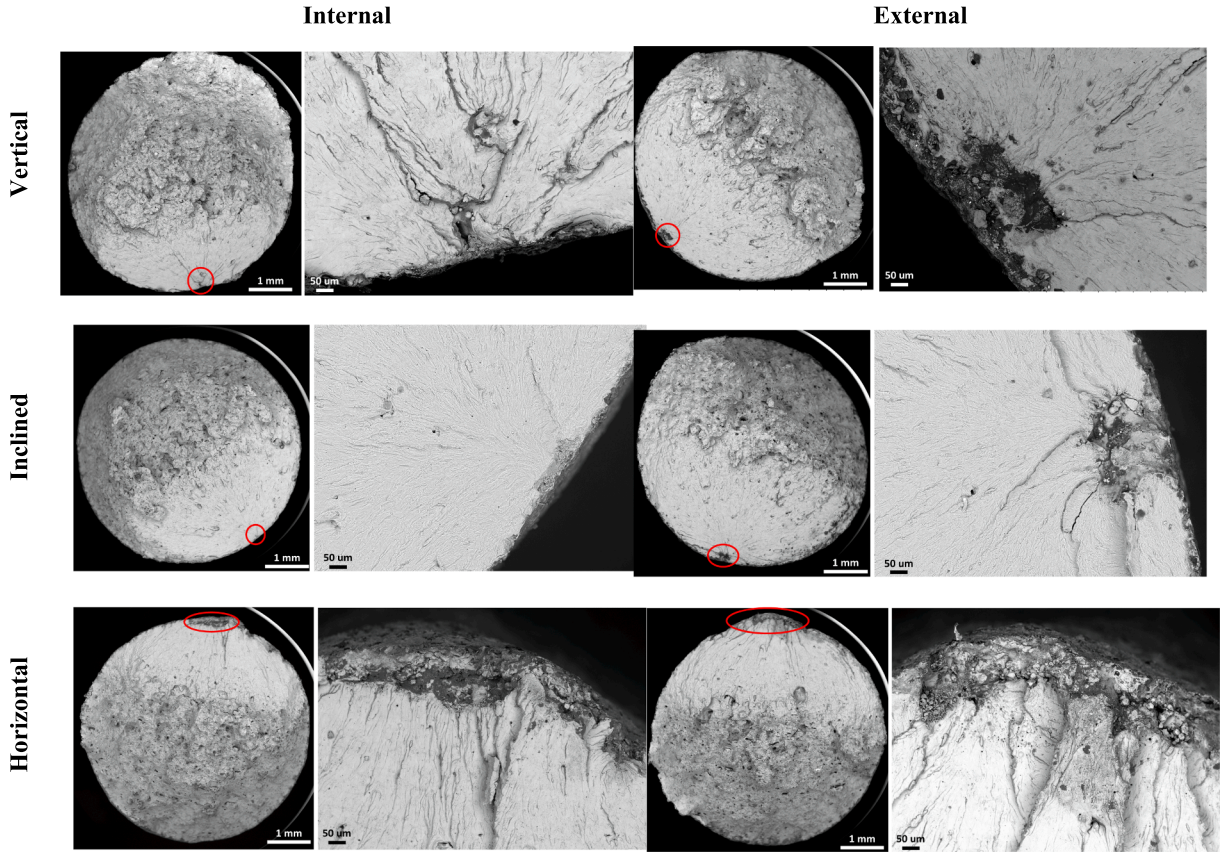

Fig. 9. Representative fracture surfaces of fatigue specimens for each combination of orientation and location. The initiation site is indicated with a red circle. (For interpretation of the references to color in this figure legend, the reader is referred to the web version of this article.)

the horizontal specimens. The fractographic analysis confirmed the MANOVA results as the failure of horizontal specimens was due to surface irregularities caused by supports. The surface quality has more influence on the fatigue properties than the expected anisotropies induced in the material by the LPBF process.

The size of the crack initiation discontinuity was determined by the square root of the defect projected area, ($\sqrt{\text{Area}}$). Fig. 10 a) shows the relationship between $\sqrt{\text{Area}}$ and the number of cycles to failure. The defect size for external specimens is slightly larger than internal specimens, 200 μm, and 165 μm. The two largest defects (500 μm and 350 μm) were found in the external position, and as expected, the corresponding cycles to failure are the lowest (497 cycles and 34,642 cycles, respectively). As the defect size decreased, the results in terms of fatigue life became homogeneous, and it was not possible to distinguish the effect of the position. This result is in accordance with the MANOVA analysis, where the coefficient β_0 is influenced by the location, meaning that external samples show lower fatigue properties because they are characterized by larger porosity.

The effect of discontinuities on fatigue can be modeled calculating the maximum stress intensity factor K_{Imax} according to the well-known model proposed by Murakami [36]:

$$K_{Imax} = Y\sigma'\sqrt{\left(\pi\sqrt{Area}\right)} \tag{4}$$

where Y is a geometrical factor, equal to 0.65 for surface defects, and σ' is the maximum stress. As shown before, horizontal specimens all

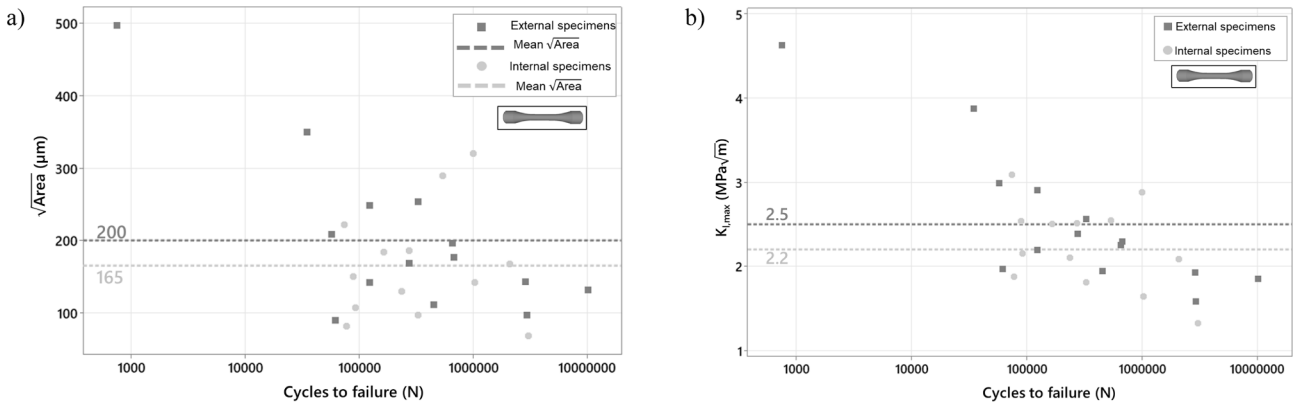

Fig. 10. Relationship between a) defect size, b) Maximum stress intensity K_{Imax} factor and cycles to failure for horizontal specimen.

failed at surface, so Y is set at 0.65 for all calculations and K_{Imax} is plotted in Fig. 10. The stress intensity factor values for internal and external specimens confirms that higher K_{Imax} are observed for external specimens in correspondence with larger defects, the mean value for the external position is 2.5 MPa $\sqrt{m}$ while for the internal is 2.2 MPa $\sqrt{m}$. At higher cycles, the differences between internal and external specimens were negligible and the values of K_{Imax} were in the range of 1–3 MPa $\sqrt{m}$, coherently with literature [44]. K_{Imax} lower bound represents the crack threshold of the material, and based on the results in Fig. 10 b), it is close to 1 coherent with literature [44].

5. Discussion

Prior to a detailed discussion regarding the effects of the batch related parameters, the results of the present work were compared to the literature data on conventionally machined specimens and other works using LPBF (Table 9). The few works available on AlSi7Mg0.6 alloy show a large variability of the fatigue properties. Rao et al. [31]obtained a fatigue limit of 200 MPa using optimized process parameters with machined specimens. The fatigue data from [30] and [27] are similar and comparable with the ones presented in this paper. The as-built results from the literature are slightly lower than the ones of the present study, this performance could be ascribed to the sand-blasting operation that is known to induce beneficial compressive stresses that resulted in improvement in the fatigue life for Al-alloys ([28,33]). LPBF fatigue data outperform the casting result for the same alloy [32].

The overall results show that a systematic influence of production batch related parameters exist on the mechanical properties of LPBF produced Al-alloy. Such influences were revealed through fatigue testing, while the conventionally used tensile testing did not reveal any significant influence of the build number or part position, while it confirmed the well-known influence of the part orientation. Hence, it can be underlined that while tensile testing can be used to confirm LPBF system capability and stability, it may not always be able to indicate the systematic influence of position and build number. It should also be emphasized that the use of correct statistical tools both in the experimental design and analysis is essential to reveal such nuances. Accordingly, the present work provides a framework beyond the results demonstrated.

Table 9
Literature results of fatigue life for AlSi7Mg0.6 alloy.

Reference	Fatigue test procedure	Specimens type and HT	Build direction	Fatigue life
[30]	R = 0.1 Frequency 100 Hz	Machined and HT (solution treatment) As-built	Vertical	175 MPa 100 MPa
[18]	R = 0 Frequency 5 Hz	As-built	Vertical	65 MPa
[31]	R = 0.1 Frequency 20 Hz	Machined and HT (T6) As-built and HT	Vertical	200 MPa 100 MPa
[27]	R = 0.1 Frequency 80 Hz	Machined and HT (T6)	Vertical	152 ± 8 MPa
[32] (Casting)	R = 0.1 Frequency 110 Hz	Machined and HT (T6)	-	103 ± 5 MPa

The results shown in this work indicate that the external specimens indeed suffer from a more critical level of defectiveness reducing their fatigue life independently from the orientation. Such issue may be related to the specific gas flow of the LPBF system as well as the processed material type. Indeed, a large fraction of the bigger defects was found to indicate spatter induced lack-of-adherence [45]. The spatter generation and its evacuation are related to the employed process parameters as well as the design of the gas flow system [39]. With lighter alloys such as the Al-alloy powder used in this work, the gas flow can be more difficult to manage. While with heavier steel or Ni-alloy powders the increase of the gas flow rate may be a solution, in the case of Al-alloys this can result in powder blow and an irregular powder bed [46]. The use of higher powder dosage or multiple wiper passages may provide a solution to improve the powder bed homogeneity. However, the powder blow may occur during the laser scanning stage [47] and an overall decay in productivity is expected due to the increased recoating time. Another remedy can be through the post-processing stage where hot isostatic pressing (HIP) can be an envisaged solution. The use of HIP with LPBF produced Al-alloys can allow to close the internal porosity, while the entrapped gases in the pores may remain an issue. Moreover, an overall reduction of the mechanical properties can be expected due to the grain coarsening [48].

The different mechanical properties with respect to the part orientation indeed indicates direction dependant material properties. In the present study, horizontal specimens resulted in lower mechanical properties contrary to the literature results, where horizontally built samples show an increased fatigue life compared to vertical ones [34] due to the anisotropy induced in the microstructure during the building process. The sandblasting process resulted in similar mean surface roughness values as displayed in Fig. 5 b), and therefore no differences in fatigue life should be expected. However, the fatigue life is supposed to be more influenced by the depth of lowest surface valley (R_z) rather than R_a [35,36] and this could explain the different mechanical performances even when the measurements of surface quality are similar among the different orientations.

It is further highlighted that direction dependant material properties should be implemented at a design stage during the topological optimization of the designed part [49]. The results of this work imply that at the topological optimization stage the part orientation in the machine

should also consider the variability of mechanical properties within the part as a function of its placement on the build platform. For multiple parts built together the solution may be straight forward possibly varying the part geometry depending on the part position. For single and large parts extending over the entire build platform the topological optimization tool may also consider location dependant properties varying the geometry accordingly.

While the work shows that systematic differences may occur within and between the LPBF build jobs, the restriction of their influence also relies on in-process defect prevention and correction strategies. In-situ monitoring approaches may be incorporated to the identification of spatter, gas [50], and powder bed irregularity issues [51], which will be essentially important when the geometrical variety of the parts produced with LPBF is concerned. The use of laser remelting [52] or layer removal and re-deposition [53] techniques have been demonstrated in literature, which may find their use from this perspective.

6. Conclusions

This work studied the influence of batch-to-batch variability as well as influence of the part orientation and position on the mechanical properties of the LPBF processed AlSi7Mg0.6 alloy. The work showed the detailed experimental with complete randomization of the static and tensile test specimens over 3 build jobs. The overall results can be summarized as follows.

- No relevant influence of the production batch related parameters on the static mechanical properties could be observed. This implies that the nuances created by the uncontrolled factors are small to have an influence of the tensile properties, or inversely tensile testing is not able to reveal such differences.
- The fatigue tests confirmed the influence of the part orientation on the stress-relieved and sandblasted AlSi7Mg0.6 specimens. The horizontal specimens were found to have the lowest fatigue life, which may be related to defects size around the support zones.
- The influence of the part position was confirmed via the fatigue data, where the external samples were characterized by a reduced fatigue life. This was attributed to the specific gas management and powder recoating system of the employed machine, possibly influencing the spatter generation and deposition during the process.
- The fractographs showed that the defects were commonly initiated around the sample edges. For vertical and inclined specimens these regions corresponded to the sub-surface lack of fusion and spatter induced adherence defects. For horizontal specimens the defects were always found around the supporting regions with typical defect sizes larger than the layer thickness which resulted in a reduced fatigue life compared to vertical and inclined orientations. As suggested by the literature, the mean surface roughness indicator might not be suitable for the prediction of the fatigue life of the specimens. The extensive presence of support structure results in the formation of sub-surface defects which must be removed with additional postprocessing, such as milling.

The present work shows a systematic investigation resolving the tackled systematic batch related factors as well as providing insights to how they may be possibly resolved. An open research question regards the variability between different feedstocks, machines of the same and different manufacturers, which is beyond the current scope. Standardization efforts and inter-laboratory collaborations are expected to facilitate such activities, which are expected to be crucial for the aerospace industry.

CRediT authorship contribution statement

Stefania Cacace: Conceptualization, Formal analysis, Writing – original draft. **Ali Gökhan Demir:** Conceptualization, Methodology, Writing – original draft. **Giuseppe Sala:** Writing – review & editing. **Antonio Mattia Grande:** Conceptualization, Investigation, Formal analysis, Methodology, Writing – original draft.

Declaration of Competing Interest

The authors declare that they have no known competing financial interests or personal relationships that could have appeared to influence the work reported in this paper.

Data availability

Data will be made available on request.

Acknowledgements

This research has been supported by the European Horizon 2020 CleanSky2 Programme, project AMATHO (Additive MAnufacturing of Tiltrotor HOusing) - GAP N° 717194.

References

[1] Kadir AZA, Yusof Y, Wahab MS. Additive manufacturing cost estimation models—a classification review. Int J Adv Manuf Technol 2020;107:4033–53. https://doi.org/10.1007/s00170-020-05262-5.
[2] Huang DJ, Li H. A machine learning guided investigation of quality repeatability in metal laser powder bed fusion additive manufacturing. Mater Des 2021;203:109606. https://doi.org/10.1016/j.matdes.2021.109606.
[3] Dowling L, Kennedy J, O'Shaughnessy S, Trimble D. A review of critical repeatability and reproducibility issues in powder bed fusion. Mater Des 2020;186:108346. https://doi.org/10.1016/j.matdes.2019.108346.
[4] Gordon JV, Narra SP, Cunningham RW, Liu He, Chen H, Suter RM, et al. Defect structure process maps for laser powder bed fusion additive manufacturing. Addit Manuf 2020;36:101552.
[5] Liu R, Liu S, Zhang X. A physics-informed machine learning model for porosity analysis in laser powder bed fusion additive manufacturing. Int J Adv Manuf Technol 2021;113:1943–58. https://doi.org/10.1007/s00170-021-06640-3.
[6] Oliveira JP, LaLonde AD, Ma J. Processing parameters in laser powder bed fusion metal additive manufacturing. Mater Des 2020;193:1–12. https://doi.org/10.1016/j.matdes.2020.108762.
[7] Liu J, Li G, Sun Q, Li Hu, Sun J, Wang X. Understanding the effect of scanning strategies on the microstructure and crystallographic texture of Ti-6Al-4V alloy manufactured by laser powder bed fusion. J Mater Process Technol 2022;299:117366.
[8] Khan HM, Karabulut Y, Kitay O, Kaynak Y, Jawahir IS. Influence of the post-processing operations on surface integrity of metal components produced by laser powder bed fusion additive manufacturing: a review. Mach Sci Technol 2021;25:118–76. https://doi.org/10.1080/10910344.2020.1855649.
[9] Cacace S, Semeraro Q. Influence of the atomization medium on the properties of stainless steel SLM parts. Addit Manuf 2020;36:101509. https://doi.org/10.1016/j.addma.2020.101509.
[10] Gibbons DW, Serfontein JPL, van der Merwe AF. Mapping the path to certification of metal laser powder bed fusion for aerospace applications. Rapid Prototyp J 2021;27:355–61. https://doi.org/10.1108/RPJ-07-2020-0154.
[11] Montgomery DC. Design and analysis of experiments. 10th ed. John wiley & sons; 2019.
[12] Thijs L, Kempen K, Kruth JP, Van Humbeeck J. Fine-structured aluminium products with controllable texture by selective laser melting of pre-alloyed AlSi10Mg powder. Acta Mater 2013;61:1809–19. https://doi.org/10.1016/j.actamat.2012.11.052.
[13] Rao JH, Zhang Y, Fang X, Chen Y, Wu X, Davies CHJ. The origins for tensile properties of selective laser melted aluminium alloy A357. Addit Manuf 2017;17:113–22. https://doi.org/10.1016/j.addma.2017.08.007.
[14] Rao H, Giet S, Yang K, Wu X, Davies CHJ. The influence of processing parameters on aluminium alloy A357 manufactured by Selective Laser Melting. Mater Des 2016;109:334–46. https://doi.org/10.1016/j.matdes.2016.07.009.
[15] Aversa A, Lorusso M, Trevisan F, Ambrosio E, Calignano F, Manfredi D, et al. Effect of Process and Post-Process Conditions on the Mechanical Properties of an A357 Alloy Produced via Laser Powder Bed Fusion. Metals (Basel) 2017;7(2):68.
[16] Trevisan F, Calignano F, Lorusso M, Pakkanen J, Ambrosio EP, Mariangela L, et al. Effects of heat treatments on A357 alloy produced by selective laser melting. In: World PM 2016 Congr Exhib; 2016. p. 1–7.
[17] Kumar MS, Javidrad HR, Shanmugam R, Ramoni M, Adediran AA, Pruncu CI. Impact of Print Orientation on Morphological and Mechanical Properties of L-PBF Based AlSi7Mg Parts for Aerospace Applications. Silicon 2021. https://doi.org/10.1007/s12633-021-01474-w.
[18] Bassoli E, Denti L, Comin A, Sola A, Tognoli E. Fatigue Behavior of As-Built L-PBF A357.0 Parts. Metals (Basel) 2018;8:634.;8(8):634.

[19] Del Re F, Contaldi V, Astarita A, Palumbo B, Squillace A, Corrado P, et al. Statistical approach for assessing the effect of powder reuse on the final quality of AlSi10Mg parts produced by laser powder bed fusion additive manufacturing. Int J Adv Manuf Technol 2018;97(5-8):2231–40.
[20] Soltani-Tehrani A, Pegues J, Shamsaei N. Fatigue behavior of additively manufactured 17–4 PH stainless steel: The effects of part location and powder re-use. Addit Manuf 2020;36:101398.
[21] Wang F. Mechanical property study on rapid additive layer manufacture Hastelloy® X alloy by selective laser melting technology. Int J Adv Manuf Technol 2012;58:545–51. https://doi.org/10.1007/s00170-011-3423-2.
[22] Zhang S, Rauniyar S, Shrestha S, Ward A, Chou K. An experimental study of tensile property variability in selective laser melting. J Manuf Process 2019:1–10. https://doi.org/10.1016/j.jmapro.2019.03.045.
[23] Cacace S, Semeraro Q. Improvement of SLM Build Rate of A357 alloy by optimizing Fluence. J Manuf Process 2021;66:115–24. https://doi.org/10.1016/j.jmapro.2021.03.043.
[24] Johnson RA, Wichern DW. Applied multivariate statistical analysis, vol. 5. NJ: Prentice hall Upper Saddle River; 2002.
[25] Grande AM, Cacace S, Demir AG, Sala G. Fracture and fatigue behaviour of AlSi7Mg0. 6 produced by Selective Laser Melting: effects of thermal-treatments. 25th Conf. Ital. Assoc. Aeronaut. Astronaut. (AIDAA 2019), AIDAA; 2019, p. 1138–44.
[26] Denti L. Additive manufactured A357. 0 samples using the laser powder bed fusion technique: Shear and tensile performance. Metals (Basel) 2018;8:670.;8(9):670.
[27] Bonneric M, Brugger C, Saintier N. Effect of hot isostatic pressing on the critical defect size distribution in AlSi7Mg0.6 alloy obtained by selective laser melting. Int J Fatigue 2020;140:105797.
[28] Nasab MH, Giussani A, Gastaldi D, Tirelli V, Vedani M. Effect of surface and subsurface defects on fatigue behavior of AlSi10Mg alloy processed by laser powder bed fusion (L-PBF). Metals (Basel) 2019;9:7–10. https://doi.org/10.3390/met9101063.
[29] Sanaei N, Fatemi A. Analysis of the effect of surface roughness on fatigue performance of powder bed fusion additive manufactured metals. Theor Appl Fract Mech 2020;108:102638. https://doi.org/10.1016/j.tafmec.2020.102638.
[30] Yang KV, Rometsch P, Jarvis T, Rao J, Cao S, Davies C, et al. Porosity formation mechanisms and fatigue response in Al-Si-Mg alloys made by selective laser melting. Mater Sci Eng A 2018;712:166–74.
[31] Rao JH, Zhang Y, Huang A, Wu X, Zhang K. Improving fatigue performances of selective laser melted Al-7Si-0.6Mg alloy via defects control. Int J Fatigue 2019;129:105215.
[32] Serrano-Munoz I, Buffiere JY, Verdu C, Gaillard Y, Mu P, Nadot Y. Influence of surface and internal casting defects on the fatigue behaviour of A357–T6 cast aluminium alloy. Int J Fatigue 2016;82:361–70. https://doi.org/10.1016/j.ijfatigue.2015.07.032.
[33] Pola A, Battini D, Tocci M, Avanzini A, Girelli L, Petrogalli C, et al. Evaluation on the fatigue behavior of sand-blasted AlSi10Mg obtained by DMLS. Frat Ed Integrita Strutt 2019;13:775–90. https://doi.org/10.3221/IGF-ESIS.49.69.
[34] Shrestha R, Simsiriwong J, Shamsaei N, Thompson SM, Bian L. Effect of build orientation on the fatigue behavior of stainless steel 316L manufactured via a laser-powder bed fusion process. Solid Free Fabr 2016 Proc 27th Annu Int Solid Free Fabr Symp - An Addit Manuf Conf SFF 2016 2016:605–16.
[35] Persenot T, Burr A, Martin G, Buffiere JY, Dendievel R, Maire E. Effect of build orientation on the fatigue properties of as-built Electron Beam Melted Ti-6Al-4V alloy. Int J Fatigue 2019;118:65–76. https://doi.org/10.1016/j.ijfatigue.2018.08.006.
[36] Murakami Y. Metal fatigue: effects of small defects and nonmetallic inclusions. Academic Press; 2019.
[37] Greitemeier D, Dalle Donne C, Syassen F, Eufinger J, Melz T. Effect of surface roughness on fatigue performance of additive manufactured Ti–6Al–4V. Mater Sci Technol (United Kingdom) 2016;32:629–34. https://doi.org/10.1179/1743284715Y.0000000053.
[38] Witkin DB, Patel D, Albright TV, Bean GE, McLouth T. Influence of surface conditions and specimen orientation on high cycle fatigue properties of Inconel 718 prepared by laser powder bed fusion. Int J Fatigue 2020;132:105392. https://doi.org/10.1016/j.ijfatigue.2019.105392.
[39] Ferrar B, Mullen L, Jones E, Stamp R, Sutcliffe CJ. Gas flow effects on selective laser melting (SLM) manufacturing performance. J Mater Process Technol 2012;212:355–64. https://doi.org/10.1016/j.jmatprotec.2011.09.020.
[40] Beevers E, Brandão AD, Gumpinger J, Gschweitl M, Seyfert C, Hofbauer P, et al. Fatigue properties and material characteristics of additively manufactured AlSi10Mg – Effect of the contour parameter on the microstructure, density, residual stress, roughness and mechanical properties. Int J Fatigue 2018;117:148–62.
[41] Mancisidor AM, Garciandia F, Sebastian MS, Álvarez P, Díaz J, Unanue I. Reduction of the Residual Porosity in Parts Manufactured by Selective Laser Melting Using Skywriting and High Focus Offset Strategies. Phys Procedia 2016;83:864–73. https://doi.org/10.1016/j.phpro.2016.08.090.
[42] Bagherifard S, Beretta N, Monti S, Riccio M, Bandini M, Guagliano M. On the fatigue strength enhancement of additive manufactured AlSi10Mg parts by mechanical and thermal post-processing. Mater Des 2018;145:28–41. https://doi.org/10.1016/j.matdes.2018.02.055.
[43] Buchbinder D, Meiners W, Pirch N, Wissenbach K, Schrage J. Investigation on reducing distortion by preheating during manufacture of aluminum components using selective laser melting. J Laser Appl 2014;26(1):012004.
[44] Martins LFL, Provencher PR, Brochu M, Brochu M. Effect of platform temperature and post-processing heat treatment on the fatigue life of additively manufactured alsi7mg alloy. Metals (Basel) 2021;11. https://doi.org/10.3390/met11050679.
[45] Koutiri I, Pessard E, Peyre P, Amlou O, De Terris T. Influence of SLM process parameters on the surface finish, porosity rate and fatigue behavior of as-built Inconel 625 parts. J Mater Process Technol 2018;255:536–46. https://doi.org/10.1016/j.jmatprotec.2017.12.043.
[46] Wen P, Qin Yu, Chen Y, Voshage M, Jauer L, Poprawe R, et al. Laser additive manufacturing of Zn porous scaffolds: Shielding gas flow, surface quality and densification. J Mater Sci Technol 2019;35(2):368–76.
[47] Demir AG, Monguzzi L, Previtali B. Selective laser melting of pure Zn with high density for biodegradable implant manufacturing. Addit Manuf 2017;15:20–8. https://doi.org/10.1016/j.addma.2017.03.004.
[48] Uzan NE, Shneck R, Yeheskel O, Frage N. Fatigue of AlSi10Mg specimens fabricated by additive manufacturing selective laser melting (AM-SLM). Mater Sci Eng A 2017;704:229–37. https://doi.org/10.1016/j.msea.2017.08.027.
[49] Smith J, Xiong W, Yan W, Lin S, Cheng P, Kafka OL, et al. Linking process, structure, property, and performance for metal-based additive manufacturing: computational approaches with experimental support. Comput Mech 2016;57(4):583–610.
[50] Repossini G, Laguzza V, Grasso M, Colosimo BM. On the use of spatter signature for in-situ monitoring of Laser Powder Bed Fusion. Addit Manuf 2017;16:35–48. https://doi.org/10.1016/j.addma.2017.05.004.
[51] Kanko JA, Sibley AP, Fraser JM. In situ morphology-based defect detection of selective laser melting through inline coherent imaging. J Mater Process Technol 2016;231:488–500. https://doi.org/10.1016/j.jmatprotec.2015.12.024.
[52] Demir AG, Previtali B. Investigation of remelting and preheating in SLM of 18Ni300 maraging steel as corrective and preventive measures for porosity reduction. Int J Adv Manuf Technol 2017;93:2697–709. https://doi.org/10.1007/s00170-017-0697-z.
[53] Colosimo BM, Grossi E, Caltanissetta F, Grasso M. Penelope: A Novel Prototype for In Situ Defect Removal in LPBF. JOM 2020;72:1332–9. https://doi.org/10.1007/s11837-019-03964-0.